Piezocapacitance measurements of phosphorous- and antimony-doped silicon: Uniaxial strain-dependent donor polarizabilities*

H. S. Tan† and T. G. Castner
University of Rochester, Rochester, New York 14627
(Received 4 August 1980)

Piezocapacitance measurements on high-purity Si, P-doped Si ($N_D \sim 6.8\times10^{16}$/cm^3 to 1.9×10^{18}/cm^3), and Sb-doped Si ($N_D \sim 6.3\times10^{16}$/cm^3) samples, with an uniaxial tensile stress applied along [110] and [100] axes and electric field along the [001] axis, were made from $T = 4.2$ to 1.1 K with a low-frequency three-terminal capacitance bridge. A value of $\epsilon_h = 11.40\pm0.06$ is obtained for the static dielectric of pure Si as $T\to0$. $\epsilon_{h,zz}$ varies linearly with a [110] axis stress σ_s for σ_s up to 610 kg/cm^2 and yields $(1/\epsilon_{h,zz})\Delta\epsilon_{h,zz}/\Delta\sigma_s = -(3.37\pm0.07)\times10^{-7}$ kg^{-1} cm^2. The temperature variation obtained was $(1/\epsilon_h)d\epsilon_h/dt = (1.12\pm0.05)\times10^{-4}$ K^{-1}. The stress-dependent $\epsilon_{zz}(N_D,x_{100})$ values always showed a minimum for a reduced valley strain $x_{100}^{\min}$ in the range 0.4 to 0.6 for Si:P and $x_{100}^{\min}\approx0.9$ for Si:Sb. For a [110] stress there was no evidence of a minimum for x_{110} up to 0.5. Values of $\alpha_D(N_D,x)$ were obtained from the Clausius-Mossotti relationship. The stress-dependent behavior of $\epsilon(N_D,x)$ and $\alpha_D(x)$ is very similar. The initial slopes are donor dependent and such that $[1/\alpha_D(0)]d\alpha_D/dx_{110}\approx2[1/\alpha_D(0)]\,d\alpha_D/dx_{100}$ in agreement with theory. For Si:P $[1/\alpha_D(0)]d\alpha_D/dx_{100} = -0.13\pm0.01$ while for Si:Sb $[1/\alpha_D(0)]d\alpha_D/dx_{100} = -0.07$. For Si:P the position of the minimum $x_{100}^{\min}$ seems to decrease slightly with increasing donor density N_D. The valley repopulation model, including valley-dependent changes in the Bohr radius with strain, cannot explain the $\alpha_D(x)$ results quantitatively. However, the data can be explained quantitatively if a strain-dependent variation of the valley-valley coupling matrix is also included. Reliable values of $\alpha_D(N_D,\omega,T=0,x=0)$ were obtained by extrapolating the finite-T data to $T=0$. The dilute-limit values of $\alpha_D(T=0)$ approximating the isolated donor polarizabilities are $(1.2\pm0.2)\times10^5$ Å^3 and $(1.9\pm0.6)\times10^5$ Å for P and Sb, respectively. $\alpha_D(N_D,T=0)$ shows an enhancement with increasing N_D, but the enhancement is less than inferred from previous work. The related stress-dependent ac conductivity data have not been analyzed quantitatively, but agree qualitatively with the dielectric constant polarizability data.

I. INTRODUCTION

In the study of magnetic or liquid-gas phase transitions, temperature is the independent variable that can be employed to sweep through the transition. On the other hand, for the insulator-metal transition (Mott transition) of one-electron impurity systems one would like to vary the density of one-electron atoms or impurities with the temperature at 0 K. For doped semiconductors and other impurity-host systems, externally applied variables such as magnetic fields,[1-4] hydrostatic pressure,[5] and uniaxial stress[6-9] can be utilized to pass through the transition. These experiments have focused on the magneto- or piezo-resistance behavior of these doped systems. More recently there has been substantial interest in the dielectric behavior[10-13] associated with the transition (at an impurity concentration N_c) as the transition is approached from the insulating side. These results for n-type silicon have shown that the static low-temperature dielectric constant $\epsilon(N)$ increases much more rapidly than predicted by Clausius-Mossotti behavior. The effective polarizability $\alpha(N)$ increases rapidly as $N\to N_c$. In the present work we investigate how the dielectric constant $\epsilon(N)$, and thus $\alpha(N)$, vary with a tensile uniaxial stress employing piezocapacitance measurements.

The uniaxial stress technique has frequently been employed in the study of the electronic properties of doped semiconductors. Since the pioneering piezoresistance measurements of Smith,[14] studies by many groups of the piezoresistance on both n-type and p-type semiconductors have been made. The early work, mostly in the higher temperature region, where the donors and/or acceptors are ionized, has been reviewed by Keyes.[15] Some of the more recent work, particularly the low-temperature work, has been discussed by Fritzsche[16] and Chroboczek.[17] Of particular relevance to the present work are the low-temperature n-type Ge results of Fritzsche[6] showing the nonmonotonic behavior of $\Delta\rho/\rho$ with stress that depends on the donor species. Combined uniaxial stress-ESR experiments have yielded information on the g-tensor components[18] $g_{\parallel}$ and $g_{\perp}$, piezohyperfine coupling constants,[19] and the stress dependence of the electron spin-lattice relaxation rate $1/T_1(x)$.[20] Hensel *et al.*[21] investigated the effects of uniaxial stress on the mass tensor of the conduction-band minima in silicon. Optical studies utilizing uniaxial stress have studied the stress-induced shift of the indirect band gap of silicon[22] and the splitting of the infrared donor transitions to the np excited states by stress.[23]

Despite the many piezoresistance, piezo-ESR, and piezo-optical studies, there appear to be few piezocapacitance studies, although the index-of-refraction n and the low-frequency dielectric con-

stant $\epsilon(N)$ have been measured as a function of hydrostatic pressure.[24] This work attempts to provide a systematic study of the dependence of the donor polarizability $\alpha(N)$ on uniaxial stress. This type of experiment yields results complementary to the piezoresistance results.[25] The Kramers-Kronig relationship implies the piezocapacitance effect ought to be related to the frequency-dependent piezoresistance.

In the past the valley repopulation model (VRM), as originally applied to the ground-state multiplet levels for n-type Ge by Price,[26] has been employed to calculate how the donor ground-state wave function is altered by an applied uniaxial stress. Wilson and Feher[18] employed the VRM to explain the stress dependence of $|\psi_D(0, x)|^2$ (x the reduced valley strain) inferred from the piezohyperfine measurements. They assumed no change in the Bohr radius a_j associated with the jth valley with uniaxial stress. However, Fritzsche[6] demonstrated from his piezoresistance studies that one needs to take account of strain-dependent valley Bohr radii $a_j(x)$ in order to quantitatively explain the piezoresistance results. Fritzsche's approach was also employed in the analysis of the piezohyperfine tensor constants obtained from ENDOR measurements.[19] The evidence for the changes in the $a_j(x)$, already substantial, is further supported by the present results on the stress-dependent donor polarizability, but these new results show that an additional correction, discussed qualitatively by Fritzsche,[6] is required to explain the $\alpha_D(x)$ results. The new correction is a logical consequence of changes in the valley Bohr radii with stress. This new correction is the change in the various valley-valley coupling matrix elements with stress resulting from stress-induced changes in the valley envelope functions.

The present investigation has also yielded more reliable values of the low-temperature asymptotic effective polarizabilities $\alpha_D(N, T \to 0)$ for Si : P and Si : Sb than obtained in earlier work.[26] The value of $\alpha_D(N \to 0, T \to 0)$ for P donors in Si is now in good agreement with a value obtained by Capizzi *et al.*[13] Having a more reliable value of the isolated donor polarizability, which is smaller than previously thought, permits one to more accurately assess the deviations from standard Clausius-Mossotti behavior as $N \to N_c$.

In Sec. II we develop the background for the stress-induced changes in the shallow donor polarizability and dielectric constant of n-type silicon. The experimental techniques and sample preparation and characterization are discussed in Sec. III. Finally the experimental results are presented, discussed, and compared with the traditional theoretical approach utilizing the VRM and stress-induced changes in the valley Bohr radii. A new theoretical model for $\alpha_D(x)$ is presented in the following paper.

II. BACKGROUND FOR STRAIN-DEPENDENT POLARIZABILITIES AND DIELECTRIC CONSTANTS

The shallow donor 1S wave functions for Si are described by

$$\psi(\vec{r}) = \sum_{j=1} C_j F_j(\vec{r}) u_{\vec{k}_{0j}}(\vec{r}) e^{i\vec{k}_{0j}\cdot\vec{r}} , \tag{1}$$

where $u_{\vec{k}_{0j}}(\vec{r}) e^{i\vec{k}_{0j}\cdot\vec{r}}$ is the conduction-band Bloch function at the jth minimum, $F_j(\vec{r})$ is the hydrogenlike envelope function solution of the Schrödinger equation for the jth valley, and C_j is the amplitude of the donor wave function associated with the jth valley. Each valley is characterized by a mass tensor with components $m_\parallel$ and $m_\perp$ [for Si (Ref. 21) $m_\parallel = 0.9163\,m$ and $m_\perp = 0.1905\,m$] and this axial anisotropy leads to an envelope function for a z-axis valley of the form

$$F_z(\vec{r}) = \frac{1}{(\pi a^2 b)^{1/2}} \exp\left[-\left(\frac{x^2+y^2}{a^2} + \frac{z^2}{b^2}\right)^{1/2}\right]. \tag{2}$$

This oblate spheroid wave function extends further in the (x, y) plane than along z since $a > b$. This single-valley envelope function (1S-state) leads to a single-valley donor polarizability tensor with components $\alpha_\parallel$ and $\alpha_\perp$. In the effective-mass approximation (EMA) Dexter[27] has calculated $\alpha_\parallel$ and $\alpha_\perp$ for Si and finds $\alpha_\perp/\alpha_\parallel = 2.123$ and $\alpha_{\rm EMA} = \frac{1}{3}(\alpha_\parallel + 2\alpha_\perp) = 4.328 \times 10^5$ Å for an Si host static dielectric constant $\epsilon_h = 11.4$.[28]

It is sometimes useful to utilize an isotropic envelope function $F(r) = (1/\pi a^{*3})^{1/2} e^{-r/a^*}$ where a^* is the EMA isotropic Bohr radius given by $a^* = a_B \epsilon_h (m/m^*)$, where m^* is an isotropic effective mass ($m^*/m = 0.299$ for Si) chosen to yield the correct value of the EMA 1S ground-state binding energy $E_{1S\text{-EMA}} = \mathrm{Ry}(m^*/m)/\epsilon_h^2$ ($E_{1S\text{-EMA}} = 31.27$ meV for Si). This isotropic envelope function leads to a polarizability $\alpha_{\rm EMA} = \frac{9}{2}\epsilon_h a^{*3} = 4.21 \times 10^5$ Å^3 or about 2.5% less than the EMA value found by Dexter. The important strongly attractive central-cell potential significantly increases the donor binding energies, decreases the effective donor Bohr radii a_D^*, and decrease the donor polarizabilities α_D by a factor of between 2 and 5 relative to $\alpha_{\rm EMA}$. Roughly speaking the α_D scale as $\alpha_D \propto (1/E_{D\text{-}1S\text{-}A_1})^3$.

In tetrahedral (T_d) symmetry the 6 1S functions split into a 1S-A_1 orbital singlet, a 1S-E doublet, and a 1S-T_2 triplet. Since the 1S-A_1 state has a

nonzero value of $|\psi(0)|^2$ while the others have $|\psi(0)|^2 = 0$, it is the $1S\text{-}A_1$ state that is substantially lowered with respect to E_{EMA} by the strong, but short-range attractive central-cell potential. The energy splitting $(E_{1S\text{-}A_1} - E_{1S\text{-}E}) = 6\Delta$ where Δ is the valley-valley coupling matrix element between adjacent valleys on different cubic axes. The $1S\text{-}T_2$ states, lying slightly below the $1S\text{-}E$ states, play an important role in the Orbach SLR process,[29] but will play no role in uniaxial stress-induced shifts of isolated donor polarizabilities. The uniaxial stress only couples the $1S_1 - A_1$ and $1S - E_a$ states with valley admixture coefficients $C_{A_1} = 1/\sqrt{6}\,(1,1,1,1,1,1)$ and $C_{E_a} = 1/\sqrt{12}\,(-2, -2, 1, 1, 1, 1)$ (x-axis stress).

Following the treatment of Wilson and Feher,[18] and using the six-component vectors[30] for the stress σ_j and the strain u_i ($u_i - u_{\alpha\beta}$ where $u_{\alpha\beta}$ is the strain tensor) related by $u_i = S_{ij}\sigma_j$ where the S_{ij} are the elastic compliance constants, the stress-induced shift of the jth conduction-band minimum is given by[31]

$$\Delta E_c^j = \sum_{\alpha\beta} (\Xi_d\,\delta_{\alpha\beta} + \Xi_u\,k_\alpha^j\,k_\beta^j) u_{\alpha\beta}\,, \tag{3}$$

where k_α^j and k_β^j are components of the unit vector from $\vec{k} = 0$ to the minimum of the jth valley, and Ξ_d and Ξ_u are the dilatational and shear deformation potentials, respectively. The average shift of the six conduction-band minima in Si for either a [110] axis or [100] axis stress is given by $\Delta E_c^{\text{av}} = (S_{11} + 2S_{12})\sigma_s(\Xi_d + \Xi_u/3)$. In either case four valleys shift up (down) and two valleys shift down (up). Next we utilize the VRM to obtain the coefficients $C_j(x)$ as a function of the reduced valley strain x and thereby obtain the ground-state donor polarizability $\alpha_D(x)$.

A. Valley repopulation model (Refs. 18 and 26)

1. [110] stress-axis case

For this case the four $(x, -x, y, -y)$ valleys shift upward in energy an amount $x_{110}\Delta$ and the two $(z, -z)$ valleys shift downward an amount $-2x_{110}\Delta$ where $x_{110} = (S_{11} - S_{12})\Xi_u\sigma_s/6\Delta$ is the reduced valley strain ($\sigma_s > 0$ for a tensile stress). For this case the ground state $C_j(x)$ takes the form $C_j = (C_A, C_A, C_A, C_A, C_B, C_B)$ with $4C_A^2 + 2C_B^2 = 1$. Solution of the 6×6 valley-orbit coupling Hamiltonian matrix for this case leads to

$$C_A^2 = \tfrac{1}{8}\left[1 + (\tfrac{2}{3} - x)(x^2 - \tfrac{4}{3}x + 4)^{-1/2}\right], \tag{4a}$$

and

$$C_B^2 = \tfrac{1}{4}\left[1 - (\tfrac{2}{3} - x)(x^2 - \tfrac{4}{3}x + 4)^{-1/2}\right] \tag{4b}$$

for $x = x_{110}$.

2. [100] stress-axis case

For this case the two $(x, -x)$ valleys shift upward an amount $2x_{100}\Delta$ and the four $(y, -y, z, -z)$ valleys shift down an amount $-x_{100}\Delta$ where $x_{100} = (S_{11} - S_{12})\sigma_s\Xi_u/3\Delta$. For this case the ground state $C_j'(x')$ takes the form $C_j'(x') = (C_B', C_B', C_A', C_A', C_A', C_A')$. Solution of the valley-orbit coupling in this case leads to $C_A'^2$ and $C_B'^2$ of the same form as in Eqs. (4a) and (4b), but with x replaced by $-x'$ where $x' = x_{100}$.

B. Stress-dependent shallow donor polarizabilities

The donor polarizabilities will be expressed as a function of the reduced valley strain $x_{110}(x)$ or $x_{100}(x')$ for the two stress-axis cases considered above. The analysis will be within the framework of the VRM and will also include the stress dependence of the valley Bohr radius $a_j(x)$ employing the approach developed by Fritzsche.[6] In this approach a strain-dependent Bohr radius $a_j(x)$ for the jth valley is given by

$$\frac{a_j(x)}{a_j(0)} = \left(\frac{E_{\text{GS}}(0)}{E_{\text{GS}}(x) - \Delta E_c^1(x)}\right)^{1/2}, \tag{5}$$

where $\Delta E_c^j(x)$ is the shift of the jth valley with valley strain and $E_{\text{GS}}(x)$ is the coupled ground-state energy as a function of valley strain. $E_{\text{GS}}(x)$ is described in terms of E_{EMA}, the single-valley correction Λ to E_{EMA}, the adjacent valley-valley coupling Δ and $\Delta(1+\delta)$ for the opposite valley coupling. The parameters Λ, Δ, and δ for P and Sb donors,[32] along with the low-temperature Si elastic constants[33] S_{11}, S_{12}, and S_{44} and the deformation potentials are shown in Table I.

The polarizability tensor $\vec{\alpha}_j$ for the z valleys will be given by

$$\vec{\alpha}_z(x=0) = \begin{vmatrix} \alpha_\perp & 0 & 0 \\ 0 & \alpha_\perp & 0 \\ 0 & 0 & \alpha_\parallel \end{vmatrix}, \tag{6}$$

with similar permuted expressions for $\vec{\alpha}_x(x=0)$ and $\vec{\alpha}_y(x=0)$. These expressions are only rigorously correct for $x = 0$ and one must consider the quantities $\alpha_{\parallel u}$, $\alpha_{\perp u}$, $\alpha_{\parallel l}$, and $\alpha_{\perp l}$, the u standing for the valleys shifted upward by the stress and the l for the valleys shifted down to a more negative energy. The polarizability tensor $\vec{\alpha}_{D\text{-GS}}(x)$ will be given by

$$\vec{\alpha}_{D\text{-GS}}(x) = \sum_{j=1}^{6} C_j^2(x)\,\vec{\alpha}_j(x) \tag{7}$$

with $\vec{\alpha}_j(x) = f_u\,\vec{\alpha}_j(0)$ for the upper valleys and $\vec{\alpha}_j(x) = f_l\,\vec{\alpha}_j(0)$ for the lower valleys. Since $\alpha_j(x)$

TABLE I. Summary of silicon and donor parameters.

	Elastic compliance constants ($\times 10^{-13}$ dyne^{-1} cm^2) (Ref. 33)	
	Pure Si-4.2 K	Si : P ($N_D = 1.98 \times 10^{19}$ cm^{-3}) – 4.2 K
S_{11}	7.617	7.995
S_{12}	−2.127	−2.317
S_{44}	12.463	12.505

Conduction-band-valley mass tensor components—deformation potentials

$m_{\parallel} = 0.9163m$ (Ref. 21) $m_{\perp} = 0.1905m$ (Ref. 21)

$\Xi_d = -5.2 \pm 0.3$ eV[a] $\Xi_u = 8.6 \pm 0.2$ eV (Ref. 22)

	Shallow donor parameters (Refs. 23, 32)		
	6Δ (meV)	δ	Λ (meV)
P	12.95	−0.308	4.13
Sb	12.14	−0.586	2.53

[a] R. Ito, H. Kawamura, and M. Fukai, Phys. Lett. 13, 26 (1964).

$\propto [a_j(x)]^3$ the $f(x)$ factors are defined by

$$f(x) = \left(\frac{a_j(x)}{a_j(0)}\right)^3 . \tag{8}$$

In the present work the electric field is always applied along the [001] axis and the capacitance measurement after corrections determines the component ϵ_{zz} of the dielectric tensor $\tilde{\epsilon}(N_D, \omega, T)$. From the Clausius-Mossotti relationship $\tilde{\epsilon}$ is related to $\tilde{\alpha}(N_D, \omega, T)$. We employ the expression developed by Castellan and Seitz,[34] which for the scalar case is

$$\epsilon = \epsilon_h + \frac{4\pi N_D \alpha_D}{[1 - (4\pi N_D \alpha_D / 3\epsilon_h)]} . \tag{9}$$

This expression states that for a single dopant the entire change in ϵ from ϵ_h results from the shallow donors, although at finite temperatures there will be a hopping contribution of the form developed by Pollak and Geballe.[35] In this work we shall use Eq. (9) without a hopping term to obtain an effective polarizability $\alpha^{\text{eff}}_{D\text{-}zz}(N_D, \omega, T, x)$ which includes hopping. However, at sufficiently low temperatures

$$\alpha^{\text{eff}}_{D\text{-}zz}(N_D, \omega, T, x) \to \alpha_{D\text{-}zz}(N_D, \omega, T = 0, x) .$$

In the presence of compensation it is only the neutral donors with concentration $(N_D - N_A)$ that contribute to $\tilde{\epsilon}$. The polarizabilities of both ionized donors and ionized acceptors are comparable in magnitude to those of the covalently bonded Si atoms and are approximately 10^{-4} the magnitude of the neutral donors. On the other hand, it is well known that compensation can contribute importantly to the hopping conductivity and to the hopping contribution to $\alpha^{\text{eff}}_D(N_D, \omega, T, x)$. Very close to the insulator-metal transition ($N_D \to N_c$) we believe compensation will have a more significant effect on the dielectric behavior.

1. [110] stress-axis case

Using Eqs. (5)–(8) and the normalization condition $4C_A^2 + 2C_B^2 = 1$, one obtains for the tensor component $\alpha_{D,zz}(x)$ (the subscript GS will be omitted henceforth) the result

$$\alpha_{D\text{-}zz}(x) = f_l\, \alpha_{\parallel} + 4C_A^2 (f_u \alpha_{\perp} - f_l \alpha_{\parallel}) , \tag{10}$$

where $C_A^2(x)$ is given by Eq. (4a) and $f_u(x)$ and $f_l(x)$ are determined by Eqs. (5) and (8). Explicit expressions for these quantities are given in the Appendix. Note that $\alpha_{D,zz}(0) = \frac{1}{3}(\alpha_{\parallel} + 2\alpha_{\perp})$. Given explicit functional dependences for $C_A^2(x)$, $f_u(x)$, and $f_l(x)$, the experimentally determined quantity $\alpha_{D,zz}(x) - \alpha_{D,zz}(0)$ is a unique function of $\alpha_{\parallel}$ and $\alpha_{\perp}$ and can be used to determine $(\alpha_{\perp} - \alpha_{\parallel})$. This quantity combined with $\alpha_{D\text{-}zz}(0)$ will then in principle determine the individual tensor components $\alpha_{\parallel}$ and $\alpha_{\perp}$. This is readily seen for the simplified case of neglecting stress-induced changes in the Bohr radii, i.e., setting f_u and $f_l = 1$. In this case Eq. (10) becomes

$$\begin{aligned} \alpha_{D,zz}(x) &= \alpha_{\parallel} + 4C_A^2(\alpha_{\perp} - \alpha_{\parallel}) \\ &= \tfrac{1}{3}(\alpha_{\parallel} + 2\alpha_{\perp}) - (\alpha_{\perp} - \alpha_{\parallel})\left(\tfrac{2}{9}x + \tfrac{1}{18}x^2 - \tfrac{1}{81}x^3 \right. \\ &\quad \left. - \tfrac{25}{1944}x^4 \ldots\right) , \end{aligned} \tag{11}$$

where the latter form is obtained by a power series expansion of $C_A^2(x)$. For $x \ll 1$, $\alpha_{D\text{-}zz}(x) - \alpha_{D\text{-}zz}(0)$ varies linearly with x with a characteristic slope $-\frac{2}{9}(\alpha_{\perp} - \alpha_{\parallel})$. The $\frac{1}{18}x^2$ term implies a decrease of $\alpha_{D\text{-}zz}(x)$ with x steeper than linear, which is not in agreement with the experimental data. The Appendix gives an expression for

$\alpha_{D\text{-}zz}(x)$ with numerical coefficients including the $f_u(x)$ and $f_l(x)$ factors for P and Sb donors. Finally we note that $\alpha_{D,zz}(x)$ is obtained from the expression

$$\epsilon_{zz}(x)=\epsilon_{h,zz}(x)+\frac{4\pi N_D\alpha_{D,zz}(x)}{1-[4\pi N_D\alpha_{D,zz}(x)/3\epsilon_{h,zz}(x)]}, \quad (12)$$

where $\epsilon_{h,zz}(x)$ is the strain-induced change in the dielectric constant of pure Si and is obtained from measurements on high purity Si samples ($N_A-N_D<10^{13}/\mathrm{cm}^3$). For $N_D<10^{18}/\mathrm{cm}^3$ the denominator in the second term in Eq. (12) is essentially unity, the correction from the Lorentz-Lorenz correction being less than 5%.

2. [100] stress-axis case

Using Eqs. (5)–(8) and the normalization condition $2C_B'^2+4C_A'^2=1$, one obtains for the tensor component $\alpha_{D,zz}(x)$ the result

$$\alpha_{D,zz}(x')=f_u'\,\alpha_\perp+2C_A'^2[f_l'(\alpha_\perp+\alpha_\parallel)-2f_u'\,\alpha_\perp], \quad (13)$$

where $C_A'^2(x')$ is given by Eq. (4a) with x replaced by $-x'$, and $f_u'(x')$ and $f_l'(x')$ are obtained from Eqs. (5) and (8). Just as in the [110] axis case, $\alpha_{D,zz}(0)=\frac{1}{3}(\alpha_\parallel+2\alpha_\perp)$ and $\alpha_{D,zz}(x')-\alpha_{D,zz}(0)$ is a unique function of $\alpha_\parallel$ and $\alpha_\perp$ once $C_A'^2(x')$, $f_u'(x')$, and $f'(x')$ are specified. For the case f_u' and f_l' set equal to 1, Eq. (13) becomes

$$\begin{aligned}\alpha_{D,zz}(x')&=\alpha_\perp+2C_A'^2(\alpha_\parallel-\alpha_\perp)\\&=\tfrac{1}{3}(\alpha_\parallel+2\alpha_\perp)-(\alpha_\perp-\alpha_\parallel)\\&\quad\times(\tfrac{1}{9}x'-\tfrac{1}{36}x'^2-\tfrac{1}{162}x'^3+\tfrac{25}{3888}x'^4+\dots),\end{aligned} \quad (14)$$

where $C_A'^2$ has been expanded in a power series. Equation (14) is similar to Eq. (11) except for a factor of $\frac{1}{2}$, and the replacement of x by x' changes the sign of the x'^2 and x'^4 term. For small x' the linear slope of $\alpha_{D,zz}(x')-\alpha_{D,zz}(0)$ vs x' is exactly $\frac{1}{2}$ of that for the [110] case in Eq. (11). But since $x'=x_{100}=2x_{110}=2x$ the slope would be identical if plotted versus the applied stress σ_s rather than versus the reduced valley strain parameters x and x'. However, the quadratic terms in Eqs. (11) and (14) are of opposite sign. Equation (14) predicts an upward deviation from the linear decrease in $\alpha_{D,zz}(x')-\alpha_{D,zz}(0)$ as x' increases, although the predicted upward deviation is much smaller than that observed experimentally. As in the [110] axis case $\alpha_{D,zz}(x')$ is determined from the value of $\epsilon_{zz}(x')$ using Eq. (12) with x replaced by x'.

As will be shown in Sec. IV the experimental data for $\alpha_{D,zz}(x)$ and $\alpha_{D,zz}(x')$ are not in quantitative agreement with Eqs. (10) and (13) for P or Sb donors in Si. This lack of agreement results from the neglect of strain variation of the valley coupling matrix element—an effect discussed qualitatively by Fritzsche.[6] When the valley wave function changes because of changes in $a_j(x)$ or $a_j(x')$ and possibly even in the Bloch functions $u_{k0j}e^{i\vec{k}_{0j}\cdot\vec{r}}$, one will expect the valley-valley coupling matrix elements to be functions of the valley strain. Because it is difficult to calculate the matrix elements which depend critically on the central-cell potential and the core part of the valley wave functions, an empirical approach will be used to obtain the corrections for $\Delta(x)-\Delta(0)$ and $\Delta(x')-\Delta(0)$. Finally, we should observe that a theory of $\vec{\alpha}_{D\text{-}GS}(x)$ or $\vec{\alpha}_{D\text{-}GS}(x')$ can be formulated using the wave function $\psi_{D\text{-}GS}$ in Eq. (1) and the Hassé approach[36] for calculating $\vec{\alpha}_{D\text{-}GS}(x)$. This new approach avoids using the parameters $\alpha_\parallel$ and $\alpha_\perp$ and leads to a different strain-dependent $\psi_{D\text{-}GS}(x)$ than given by Eq. (1). This new, more satisfactory theoretical formulation is presented in the following paper.

III. EXPERIMENTAL PROCEDURES AND SAMPLE PREPARATION

A. Samples and sample preparation procedures

The nominally uncompensated n-type and high-purity Si samples studied in this investigation are listed in Table II. Most of the samples studied were grown by the Czochralski method although the high-purity samples and the Si:Sb samples were obtained from float zone ingots. The table shows the stress axis for each sample and the thicknesses and widths of each sample. The neutral donor concentrations were obtained from room-temperature resistivity measurements using the four-point probe method.

Rectangular slabs, approximately $0.90\times0.51\times0.22$ in. thick, were cut with a precision wafering saw from the x-ray-oriented ingots. The axis normal to the slab was chosen to be closely a [001] axis along which the electric field would be applied. The long axis of the slab was chosen as either a [100] or [110] axis and ultimately became the stress axis. The final accurate orientation of each slab was obtained using an x-ray diffraction unit attached to a Do-All $D6$ surface grinder. This allowed the rectangular block sample edges to be aligned to the Si crystallographic axes to $\pm0.25°$. The rectangular block was ground to a final size of approximately $0.84\times0.475\times0.17$ in. thickness in preparation for the final shaping.

The final shape of samples prepared to be held by the uniaxial tensile rig vises is shown in Fig.

TABLE II. Sample specifications.

Sample[a]	Stress axis	RT resistivity (ohm cm)	N_D[b] (cm^{-3})	Thickness t (mm)	Width w (cm)
*H*1*a*-High purity	[110]	750 (*p* type)	$\sim 5\times10^{13}$	0.734 ± 0.002	1.85 ± 0.001
*H*1*b*-High purity	[110]	750 (*p* type)	$\sim 5\times10^{13}$	0.626	1.177
*P*1-Phos	[100]	0.1025	6.8×10^{16}	0.383	1.199
*P*2-Phos	[110]	0.1025	6.8×10^{16}	0.504	1.202
*P*3-Phos	[100]	0.0490	2.26×10^{17}	0.663	1.187
*P*4-Phos	[110]	0.0490	2.26×10^{17}	0.522	1.164
*P*5-Phos	[100]	0.0317	5.1×10^{17}	0.498	1.223
*P*6-Phos	[110]	0.0327	4.8×10^{17}	0.656	1.200
*P*7-Phos	[100]	0.0160	1.90×10^{18}	0.553	1.217
*P*8-Phos	[110]	0.0162	1.87×10^{18}	0.517	1.186
*P*9-Phos	[100]	0.0188	1.41×10^{18}	0.667	1.191
*P*10-Phos	[110]	0.0192	1.38×10^{18}	0.447	1.197
*S*1-Phos	[100]	0.0185	1.43×10^{18}	0.538	1.198
*S*2-Phos	[110]	0.0185	1.43×10^{18}	0.639	1.170
*D*1-Sb	[100]	0.1275	6.25×10^{16}	0.412	1.190
*D*2-Sb	[110]	0.126	6.35×10^{16}	0.446	1.188
*D*3-Sb	[110]	0.130	6.1×10^{16}	0.616	1.195

[a] High performance technology (*H*), Dow-Corning (*D*)—float zone ingots Pensilco (*P*), Siltec (*S*)-Czochralski-grown ingots.

[b] N_D for Si : P samples obtained from Mousty *et al.* (Ref. 39) curve; N_D for Si : Sb samples obtained from Sze-Irvine (Ref. 40) curve.

2. The tapered ends (20° slope with respect to the sample flat) were ground with the Do-All grinder employing a special brass sample holder jig and sample holder mounting blocks, as illustrated in Fig. 1. The 20° slope on the brass saddle was machined to ± 0.1°. The two brass mounting blocks are locked in position on the jig by an alignment pin and two screws. Obtaining a smooth transition between the 20° sample slope and the sample flat was important and was achieved by fine adjustment of the goniometer head, depth of cut, and the lateral translation of the grinding wheel. The cut of the grinding wheel (and/or the relative alignment of the grinding wheel to the x-ray unit) was not "true" resulting in a slightly deeper cut at one edge than at the other. This problem, plus the surface texture left by the grinding wheel, meant the surface "flat" regions were not perfectly flat and the flat region used for the capacitance measurements was not of uniform thickness.

Shortly before evaporating Au electrodes on the samples the samples were etched with a standard CP-4 etch solution for 40 seconds to remove surface damage from grinding. The etch typically reduced uniformly the dimensions of the samples by about 0.003 in. The dimensions of the sample were then measured. The width of the samples was measured to an accuracy of 0.01 mm. However, the small thickness and the uneven surface of the sample flat region required many measurements and suitable averaging utilizing a special tapered head (0.032 in. radius) micrometer. In some instances measurements were repeated over the evaporated Au electrodes after the piezocapacitance data were obtained. The accuracy of the thickness measurements was 0.002 mm for the average sample thickness. Even this accuracy can still lead to a sizable error in the determination of $\alpha_D(N)$ in the dilute limit. Au electrodes of approximately 1200 Å thickness and 0.635 cm width were evaporated on the flat central portion of the sample as shown in Fig. 2. Mylar strips (0.002 in. thick) were glued to tapered ends of the sample to insulate it from the grounded stainless-steel vices. Copper leads were cemented to the Au electrodes with silver conducting paint.

A thin disk sample was cut from the ingot adjacent to each uniaxial stress sample for the purpose of making four-point probe resistivity measurements. The resistivity was determined by standard tables[37] and included the thickness correction factor.[38] For Si : P the neutral donor concentrations were obtained from the Mousty-Ostoja-Passori[39] curve (assumed to be more reliable than the Sze-Irvine[40] curve) while for

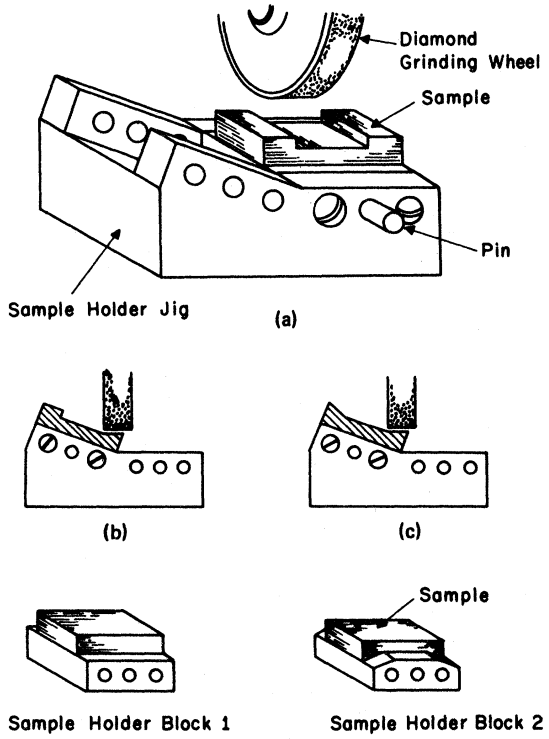

FIG. 1. Sample-shaping procedure, sample holder jig, and sample holder blocks. (a) The central portion of the sample is ground, then (b) and (c) the sample ends are ground with the sample-holder block mounted on the 20° slope of the jig. After one face is completed the sample is turned over and mounted on sample-holder block 2 to grind the second surface.

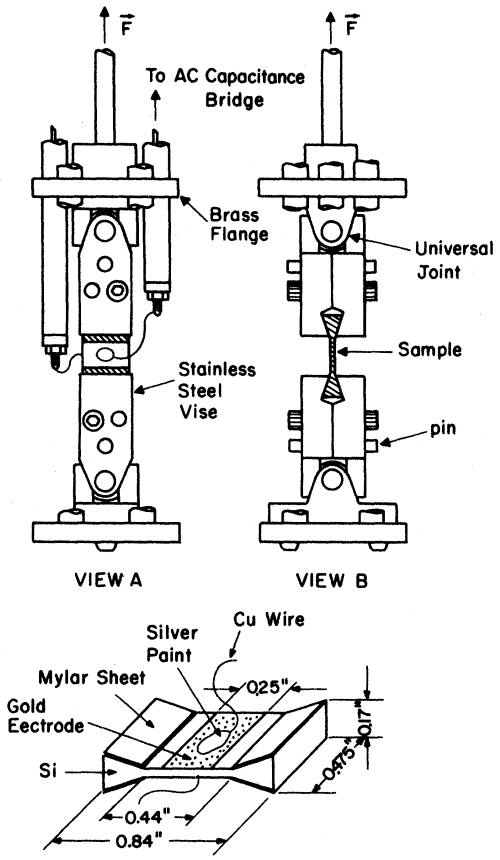

FIG. 2. Tensile stress rig with vise jaws and sample.

Si : Sb the Sze-Irvine curve was employed. The values of N_D obtained are expected to be accurate to ±7%.

B. The tensile stress rig

The lower section of the tensile stress rig is shown in Fig. 2. The upper section was constructed to five thick-walled stainless-steel tubes held rigid by a series of brass flanges. The tensile force $\vec{F}$ was applied to the upper vise and sample with a $\frac{1}{8}$-in.-diameter stainless-steel tube, which in turn was coupled to a simple lever (mechanical advantage = 5) above the top flange of the low-temperature insert. Both the upper and lower vises feature universal joints to provide "self-alignment" of the tensile force. Two of the four outer supporting stainless-steel tubes contained the electrical leads consisting of Be-Cu wires, interrupted at their midpoints by short sections of thin-walled stainless tubing for thermal insulation, connecting the sample to the three-terminal capacitance bridge. The entire lower section of the stress rig was contained inside a 1.5-in.-diam stainless-steel can which would be soldered with cerroseal to a brass flange to provide a vacuum-tight enclosure. During experiments 200–300 microns of helium exchange gas was employed to maintain the vises and sample at the liquid He bath temperature.

Strain gauges were employed to calibrate the strain produced by the tensile rig using the same approach utilized by Olson.[41] As found by Olson the strains obtained by strain-gauge measurements agreed to within 5% with the calculated strains using the standard elastic constants of Si. In this work all the strains ($u_{\alpha\beta}$) and reduced valley strains (x_{100} and x_{110}) were calculated from the known low-temperature elastic constants[33] and the applied stresses. Based on the strain-gauge results and observed hysteresis, a maximum frictional load correction of 0.17 kg was determined and applied to the data. This frictional correction was less than 2% at large loads (10 kg).

C. Piezocapacitance measurements and corrections

The capacitance measurements were made with a GR1616 three-terminal precision capacitance

bridge utilizing a PAR129A lock-in-amplifier as a detector. The stress-induced fractional capacitance changes varied from 3×10^{-5} to 5×10^{-2} (at maximum stress) from the lightly doped to more heavily doped samples. For a 40-mV ac voltage across the sample the bridge sensitivity was sufficient to detect $(\Delta C/C)$ changes of order 10^{-6}. No change in $[C(x_{\max})-C(0)]/C(0)$ was observed when the sample voltage was changed from 10 to 60 mV. The stress-dependent dielectric constant changes observed can be considered to be thermal equilibrium shifts with no measurable hot electron effects. Frequency-dependent measurements (31 Hz to 10 kHz) were both obtained at zero and maximum stress at 4.2 and 1.1 K. The stress-dependent measurements were made at the optimum frequency of 3 kHz.

In order to obtain the correct dielectric constant $\epsilon(N_D,x)$ as a function of the valley strain the following corrections had to be considered, namely (1) the geometric correction resulting from changes in the sample dimensions with stress, (2) the edge capacitance correction, (3) the Schottky barrier capacitance resulting from the depletion regions just inside the Au electrodes, and (4) the stray capacitance due to the unshielded Cu leads. To obtain the neutral donor polarizabilities $\alpha_D(N,x)$ an accurate determination of $\epsilon_h(x)$ is required. If the length (Au covered section), width, and thickness of a sample determined at room temperature (RT) are, respectively, l_0, w_0, and t_0 then the quantities $l(\sigma_s)$, $w(\sigma_s)$, and $t(\sigma_s)$ are calculated using the factor $(1-\alpha_t)$ (α_t is the thermal contraction from RT to the liquid He temperature range; $\alpha_t=2.2\times10^{-4}$ for Si) and the appropriate strain calculated from the elastic constants S_{11}, S_{12}, S_{44}, and the tensile stress σ_s ($\sigma_s=F/wt$). The two stress-axis cases, [110] and [100], led to different expressions for $l(\sigma_s)$, $w(\sigma_s)$, and $t(\sigma_s)$.

The dielectric constant ϵ_{zz} was obtained from the measured capacitance C using the expression

$$\epsilon_{zz}=(C-C_e)/(\epsilon_0 lw/t)\,, \tag{15}$$

where ϵ_0 is the permeability of free space and C_e is the edge correction capacitance of the sample. C_e is given reliably by the empirical formula[42]

$$C_e=\left[\frac{(2w+2l)}{40}\ln\left(\frac{1.5}{t}\right)+0.0185(2w\epsilon_{zz}+2l)\right]\text{pF}\,, \tag{16}$$

where l, w, and t are in cm. Equation (16) takes account of the fact that the two edges of length l are bounded by He gas ($\epsilon\simeq1$) while the two edges of length w are bounded by the doped Si with dielectric constant ϵ_{zz}. Thus, since C_e involves ϵ_{zz} one must solve Eq. (15) for ϵ_{zz}. The neglect of C_e can result in an error of 3–5% in ϵ_{zz} depending on the magnitude of N_D. The neglect of C_e would introduce a very serious error in the determination of the donor polarizability in the dilute doping limit. The Au electrodes produce depletion regions on each side of the sample resulting from the Schottky barriers. The Schottky barriers, each having a capacitance[43] $C_B=\epsilon_0 lw(e\epsilon_h N_D/2V_b)^{1/2}$, where V_b is the barrier height (for Au on Si $V_b=0.8$ eV), are in series with the sample capacitance C_s. The effective capacitance C_{eff} measured is given by

$$C_{\text{eff}}=\frac{C_sC_B}{2C_s+C_B}=\frac{\epsilon_0\epsilon lw}{t+2t_B(\epsilon/\epsilon_h-1)}\,,$$

where t is the total sample thickness and t_B is the Schottky barrier width.[43] For $N_D>10^{18}/\text{cm}^3$, $t_B<10^{-4}t$ while in the dilute limit $\epsilon\to\epsilon_h$ and the correction term in the denominator is negligible. The measured values of C_{eff}, excluding the edge correction C_e, are very accurately given by $C_{\text{eff}}\approx\epsilon_0\epsilon lw/t$.

A stray capacitance due to the unshielded copper electrical leads was difficult to accurately determine with the sample in place, but was found to be of order 0.01 pF without the sample. This results in an error of 0.07% or less in the measured capacitance. This error contributes to the absolute magnitude of $\alpha_D(N)$, but makes virtually no contribution to the stress-dependent behavior. Since this stray capacitance error is less than that due to errors in t it has been neglected.

IV. EXPERIMENTAL RESULTS AND DISCUSSION

In order to obtain stress-dependent donor polarizabilities one requires the dependence of $\epsilon_{h,zz}$ on stress, hence the results on high-purity Si will first be considered. Then results for Si:P and Si:Sb samples will be presented and the $\alpha_D(x)$ behavior will be compared with the theoretical model given in Sec. II. An additional correction taking account of strain-dependent valley-valley coupling will be considered. The extrapolated zero-temperature values of the zero-strain polarizabilities are compared with other experimental values and with theoretical values. Finally a brief discussion of the strain-dependent hopping ac conductivity results will be given.

A. High-purity Si results

The dielectric constant component $\epsilon_{h,zz}$ varies linearly with the stress σ_s up to 600 kgm/cm^2 with a slope independent of temperature in the temperature range 4.2 to 1.1 K. Measurements

were only made for a [110] stress axis and [001] electric field direction. These results yielded the result

$$[1/\epsilon_{h,zz}(0)](\Delta\epsilon_{h,zz})/(\Delta\sigma_s)$$

$$=-(3.37\pm0.07)\times10^{-7}\ \mathrm{kg^{-1}\ cm^2}.$$

From hydrostatic pressure studies Cardona *et al.*[24] have reported values of $1/\epsilon(0)(\Delta\epsilon/\Delta\sigma_{hyd})$ for pure Si to be $-(4\pm1)\times10^{-7}\,\mathrm{kg^{-1}\ cm^2}$ at 10 MHz and $T=263$ K, and $-(6\pm4)\times10^{-7}\,\mathrm{kg^{-1}\ cm^2}$ at infrared frequencies and $T=297$ K. The linear shift of the dielectric constant with strain is related to the strain by a fourth-rank tensor $\Gamma_{ij,kl}$, which at present is not well characterized experimentally. If one retains only the diagonal component $\Gamma_{ii,ii}$ of this tensor, an approximate relationship between the hydrostatic pressure and uniaxial stress shifts of ϵ is found to be

$$\frac{1}{\epsilon_h(0)}\frac{\Delta\epsilon_h}{\Delta\sigma_{hyd}}\approx-\left(\frac{S_{11}+2S_{12}}{S_{12}}\right)\frac{1}{\epsilon_{h,zz}(0)}\frac{\Delta\epsilon_{h,zz}}{\Delta\sigma_s}. \tag{17}$$

Using the values S_{11} and S_{12} from Table I, one infers the result

$$[1/\epsilon_h(0)](\Delta\epsilon_h/\Delta\sigma_{hyd})=-(5.3\pm0.3)\times10^{-7}\,\mathrm{kg^{-1}\ cm^2}$$

which is intermediate between the two RT range values obtained by Cardona *et al.* It is not obvious that there should be any temperature dependence of this quantity, and the present result may be much more accurate than the earlier results. From a dielectric constant calculation Van Vechten[44] obtained the result $(r/\epsilon_h)(d\epsilon_h/dr)=1.80$ (r the nn distance), which using $dr/r=u_{xx}=u_{yy}=u_{yy}=-(s_{11}+2s_{12})\sigma_{hyd}$ yields the results

$$[1/\epsilon_h(0)](d\epsilon_h/d\sigma_{hyd})=-6.2\times10^{-7}\ \mathrm{kg^{-1}\ cm^2},$$

slightly larger than the above value.

A plot of $\epsilon_{h,zz}(\sigma_s, T)$ vs T for three different values of the stress σ_s is shown in Fig. 3. These results ($\nu=3$ kHz data) can be extrapolated to $T=0$ K to obtain the value $\epsilon_h(\sigma_s=0, T=0)$. Despite the apparent relative accuracy of the data, the absolute accuracy of $\epsilon_h(\sigma_s=0, T=0)$ is limited by the sample thickness measurement. If the sample thickness errors plus other small systematic errors are taken into account we obtain $\epsilon_h(\sigma_s=0, T=0)=11.40\pm0.06$, which is slightly smaller than earlier experimental values obtained by refractive index measurements,[24,45-50] and by radio frequency capacitance measurements,[51] but is in excellent agreement with Faulkner's value[28] $\epsilon_h=11.40\pm0.05$ inferred from EMA theory and the energy positions of the $2p$ and $3p$ excited donor states. The earlier experimental values of n (n the refractive index, $n=\sqrt{\epsilon_h}$) and ϵ_h were obtained at $T=77$ K and higher temperatures and one expects $\epsilon_h(T)$ to increase with T. Values of $(1/n)dn/dT$ have been reported by Cardona *et al.*[24] and by Lukes[48] in the 77 K to RT range. From these results one obtains values of $[1/\epsilon_h(0)](d\epsilon_h/dT)$ of $(7.8\pm0.8)\times10^{-5}\ \mathrm{K^{-1}}$ and $(9.6\pm0.4)\times10^{-5}\ \mathrm{K^{-1}}$, respectively, which are to be compared with the result obtained from Fig. 3 at 4.2 K of $1.12\times10^{-4}\ \mathrm{K^{-1}}$. Whether this low-temperature value results from the host Si lattice or also contains residual hopping contributions from the impurities in this nominally "pure" sample is uncertain.

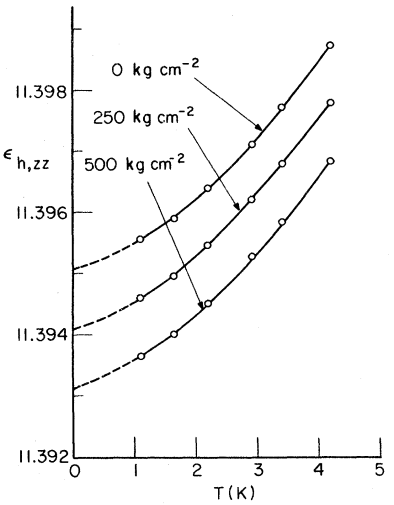

FIG. 3. Dielectric constant $\epsilon_{h,zz}$ of high-purity Si versus temperature with a [110] axis uniaxial stress as a parameter.

B. Frequency-dependent dielectric constant behavior

In Fig. 4(a) and (b) are shown the frequency-dependent dielectric constants for zero stress and at a large stress for 4.2 K and at a considerably lower temperature for a dilute sample (a) ($P3$) and a concentrated sample (b) ($P7$), respectively. For the dilute sample at both $T=4.20$ K and $T=1.126$ K there is an increasingly important frequency-dependent hopping contribution to $\epsilon_{zz}(x, T, \nu)$ for ν decreasing below 1 kHz. For $\nu>1$ kHz the $x_{100}=0$ and x_{110} large curves parallel each other at both temperatures and the strain dependence resulting from $\epsilon_{h,zz}(x)$ and $\alpha_D(x)$ is virtually the same at both temperatures. For $\nu<0.1$ kHz the strain dependence includes the hopping contribution and is smaller at $T=1.126$ K than at 4.20 K. For the $P7$ sample in Fig. 4(b) the hopping is the dominant contribution to ϵ_{zz} at

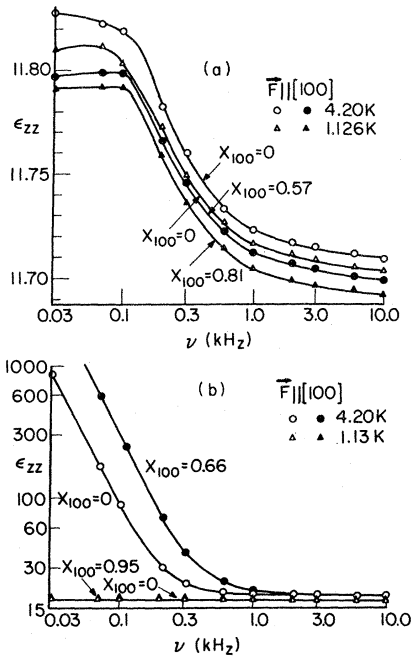

FIG. 4. Dielectric constant ϵ_{zz} versus frequency (kHz) for the valley strain $x_{100}=0$ and for a large value of x_{100}. (a) Sample $P3$ (Si:P, $N_D=2.26\times10^{17}/\text{cm}^3$) $\circ\bullet T=4.20$ K, $\triangle\blacktriangle T=1.126$ K; (b) sample $P7$ (Si:P, $N_D=1.9\times10^{18}/\text{cm}^3$) $\circ\bullet T=4.20$ K, $\triangle\blacktriangle T=1.13$ K.

low frequencies at 4.2 K. ϵ_{zz} varies as $1/\nu^2\tau^2$ for $\nu<0.2$ kHz and the strain shortens τ (increases hopping rate and σ_{AC}) by approximately a factor of two. For $\nu\gtrsim3$ kHz the hopping contribution to $\epsilon_{zz}(x)$ is very small and the dominant strain dependence, which is too small to see in the figure, results from $\epsilon_{h,zz}(x)$ and $\alpha_D(x)$. At $T=1.13$ K th frequency dependence is very small ($\Delta\epsilon_{zz}<0.1$ from $\nu=0.03$ to 10 kHz) and the hopping contribution is negligible. The two curves $\epsilon(\nu, x_{100}=0)$ and $\epsilon(\nu, x_{100}=0.95)$ are virtually parallel and the strain dependence of ϵ_{zz} results predominantly from $\epsilon_{h,zz}(x)$ and $\alpha_D(x)$. All the strain-dependent results presented in the next section are for measurements at $\nu=3.0$ kHz where the hopping contribution to $\epsilon_{zz}(x)$ is negligible at low enough temperatures and small at $T=4.2$ K.

C. Strain-dependent dielectric constants and donor polarizabilities

The strain-dependent dielectric constant values $\epsilon_{zz}(x_{110})$ and $\epsilon_{zz}(x_{100})$ versus valley strain for Si:P samples $P5$ and $P6$ ($N_D\sim5\times10^{17}/\text{cm}^5$) and $S1$ and $S2$ ($N_D=1.43\times10^{18}/\text{cm}$) are shown in Figs. 5 and 6, respectively. The ϵ_{zz} values were obtained from the measured capacitance values, Eq. (15), and the sample dimensions. The ϵ_{zz} results for the other doped-Si samples listed in Table II are qualitatively similar to the results shown in these two figures. The principal results for the strain-dependent polarizabilities of all the doped-Si samples are listed in Table III.

For the [110] axis data $\epsilon_{zz}(x)$ decreases almost linearly with x, but shows a slight upward deviation from a strictly linear drop with x. This behavior is in qualitative but not quantitative agreement with Eqs. (10) and (11). The small decrease of $\epsilon_{zz}(x)$ with temperature results from the decrease in the residual hopping contribution to $\epsilon_{zz}(x)$ with decreasing temperature. The [100] axis results

TABLE III. Summary of experimental results of doped samples.

Samples	Stress axis	$\alpha_D(x=0, T=0)$ $x(10^5A^3)$	$\frac{1}{\alpha_D(0)}\frac{\Delta\alpha_D}{\Delta x}\Big\vert_{T\to0}$	$x_{100}^{\min}$	$\left(\frac{\alpha_D(0)-\alpha_D(x_{100}^{\min})}{\alpha_D}\right)\times100$
Si:P $P1$	100	1.6±0.5	−0.15±0.02	0.40	2.6 ±0.3
$P2$	110	1.3±0.4	−0.30±0.03		
$P3$	100	1.2±0.2	−0.12±0.02	0.59	3.17±0.05
$P4$	110	1.4±0.2	−0.24±0.01		
$P5$	100	1.4±0.1	−0.12±0.01	0.59	3.15±0.05
$P6$	110	1.4±0.1	−0.24±0.01		
$P7$	100	2.1±0.1	−0.13±0.01	0.36	2.3 ±0.1
$P8$	110	2.1±0.1	−0.26±0.01		
$P9$	100	2.2±0.2	−0.13±0.01	0.42	3.0 ±0.1
$P10$	110	2.1±0.1	−0.27±0.01		
$S1$	100	2.0±0.1	−0.14±0.01	0.42	2.98±0.05
$S2$	110	2.0±0.1	−0.28±0.01		
Si:Sb $D1$	100	2.0±0.6	−0.07±0.01	0.90	2.8 ±0.2
$D2$	110	1.9±0.6	−0.14±0.01		
$D3$	110	1.9±0.6	−0.15±0.01		

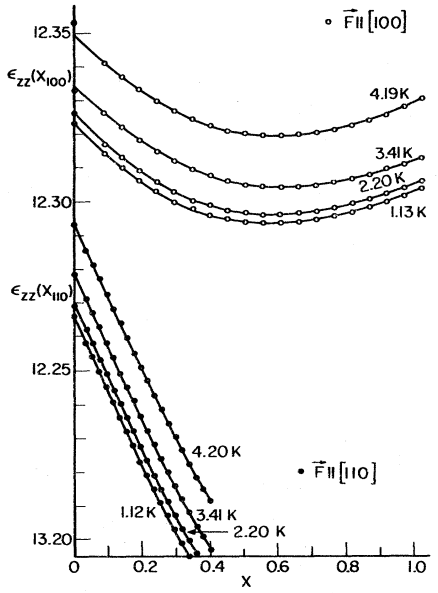

FIG. 5. Dielectric constants $\epsilon_{zz}(x_{100})$ and $\epsilon_{zz}(x_{110})$ vs x_{100} and x_{110}, respectively, for samples $P5$ (Si:P, $N_D = 5.1\times10^{17}/\text{cm}^3$) and $P6$ (Si:P, $N_D = 4.8\times10^{17}/\text{cm}^3$) for temperatures from 4.2 to 1.12 K.

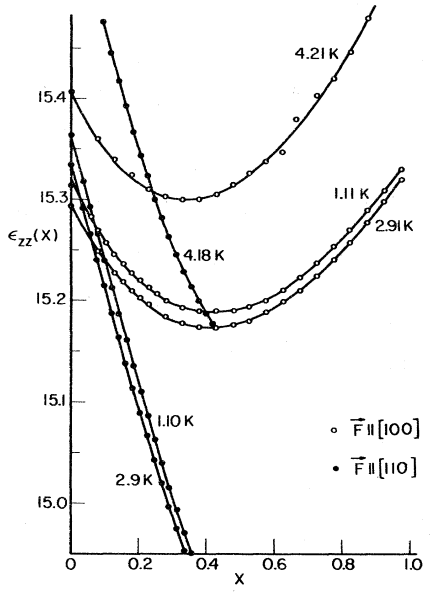

FIG. 6. Dielectric constants $\epsilon_{zz}(x_{100})$ and $\epsilon_{zz}(x_{110})$ vs x_{100} and x_{110}, respectively, for samples $S1$ (Si:P, $N_D = 1.43\times10^{18}/\text{cm}^3$) and $S2$ (Si:p, $N_D = 1.43\times10^{18}/\text{cm}^3$) for temperatures from 4.2 to 1.10 K.

for $\epsilon_{zz}(x')$ also show a decrease with x', but which exhibits a considerably smaller slope $d\epsilon_{zz}/dx'$ than the [110] axis case. In the vicinity of $x' \sim 0.6$, $\epsilon_{zz}(x')$ passes through a shallow minimum and starts to slowly increase. Again there is a small temperature dependence of $\epsilon_{zz}(x')$ from residual temperature-dependent hopping conductivity contribution to the dielectric constant. However, to a very good approximation the $\epsilon_{zz}(x', T)$ move rigidly down with decreasing temperature implying the strain-dependent $\epsilon_{zz}(x')$ behavior is virtually independent of temperature. The observation of a minimum at such small values of x' is not in agreement with the predictions of Eqs. (14) and (12) and is one of the important new results of the present work. This data will be discussed in more detail shortly after using Eq. (12) to obtain the dependence of α_D^{eff} on the valley strain.

The results in Fig. 6 for the more heavily doped Si:P sample ($N_D \sim 1.43\times10^{18}/\text{cm}^3$) show behavior qualitatively similar to the more dilute results, but with the following differences: (1) The magnitude of the $\epsilon_{zz}(x)$ values are larger, (2) the lowest temperature data (1.1 K) is slightly larger than the values at larger temperatures (2.9 K), and (3) the position of the minimum for the [100] axis case shifts with temperature, increasing as the temperature is lowered to a value $x_{100}^{\min} \approx 0.42$ which is lower than for the more dilute samples. Despite these differences the initial slopes are almost the same and are a factor of two larger for the [110] axis than for the [100] axis stress. Because of the smaller value of $x_{100}^{\min}$ the value of $\epsilon_{zz}(x' \sim 1)$ now slightly exceeds the unstressed value $\epsilon_{zz}(x' = 0)$.

Figures 7 and 8 show, from the results in Fig. 5 (but with more temperatures) using Eq. (12), the strain-dependent effective donor polarizabilities $\alpha_D(x_{100})$ and $\alpha_D(x_{110})$. These figures show virtually the same behavior as already discussed

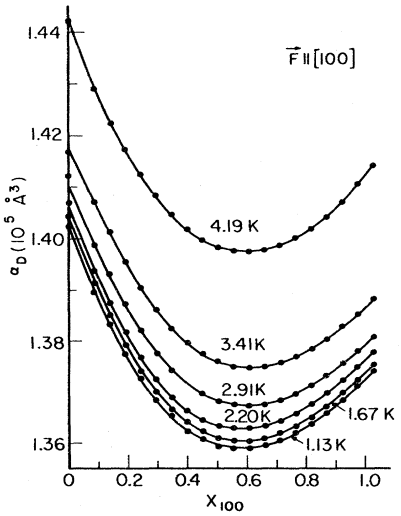

FIG. 7. The polarizability $\alpha_D(x_{100})$ vs x_{100}, for sample $P5$ (Si:P, $N_D = 5.1\times10^{17}/\text{cm}^3$) and for temperatures from 4.19 to 1.13 K, obtained from Eq. (12).

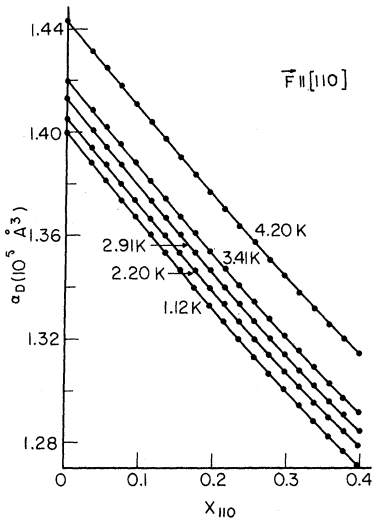

FIG. 8. The polarizability $\alpha_D(x_{110})$ vs x_{110}, for sample $P6$ (Si:P, $N_D = 4.8\times10^{17}/\text{cm}^3$) and for temperatures from 4.20 to 1.12 K, obtained from Eq. (12).

for the $\epsilon_{zz}(x)$ results in Fig. 5 and differ only because of the small linear variation of $\epsilon_{h,zz}$ with x. We also note that strain-dependent results (see Table III) for samples $P3$ and $P4$ ($N_D \sim 2.26 \times 10^{17}$ cm^{-3}) are identical to within experimental error. It is these results that will be compared with theoretical expressions given by Eqs. (10) and (13).

Figure 9 shows results for $\alpha_D(x_{100})$ for a relatively dilute Si:Sb sample ($D1$) stressed along a [100] axis. Although the strain-dependent behavior of $\alpha_D(x_{100})$ is qualitatively similar to that for the Si:P samples there are some quantitative differences. The initial slope $\{[1/\alpha_D(0)] \times (d\alpha_D/dx')\}_{x'=0}$ is almost a factor of two smaller and the position of the minimum, $x_{100}^{\min}$, has moved out to $x_{100} \sim 0.9$. These results suggest a characteristic

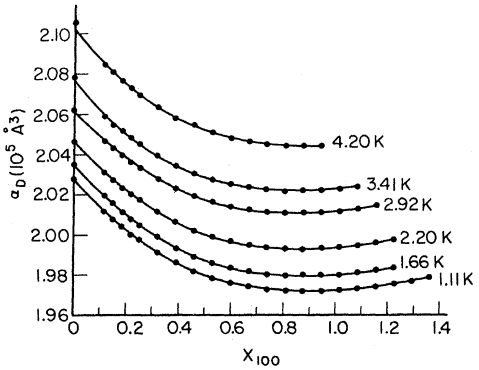

FIG. 9. The polarizability $\alpha_D(x_{100})$ vs x_{100}, for the dilute Sb sample $D1$ (Si:Sb, $N_D = 6.25\times10^{16}/\text{cm}^3$) and for temperatures from 4.20 to 1.11 K, obtained from Eq. (12).

donor-dependent behavior for $\alpha_D(x_{100})$ which, in fact, is not predicted by the VRM modified by Fritzsche's correction. Si:Sb samples $D2$ and $D3$ show characteristic [110] axis strain-dependent behavior with an initial slope which is closely twice that for the [100] axis case. These Si:Sb samples all show a temperature dependence of $\epsilon_{zz}(x, T)$ and $\alpha_D(x, T)$ resulting from the residual hopping. To a very good approximation the curves shift rigidly downward with decreasing temperature. Thus, the strain-dependent behavior is insensitive to temperature in this temperature range.

D. Comparison with the theoretical model

The [100] axis experimental data for Si:P of sample $P5$ ($P3$ would be virtually the same) is compared with the expressions given by Eqs. (13), (A2), and (14) in Fig. 10. The parameters for P donors for $a_j(x)/a_j(0)$ are obtained from Table I. The $[\text{VRM}]_{a(0)}$ curve, calculated from Eq. (14), does not take account of strain-dependent $a_j(x)$ and is in poor agreement with the experimental values of $\alpha_D(x_{100})/\alpha_D(0)$. There is no evidence of a minimum out to $x_{100} \sim 3$ and the initial slope is substantially too small. The curve $[\text{VRM}]_{a(x_{100})}$ based on Eq. (A2) includes the Bohr radius strain variation. It is in somewhat better agreement, showing a slightly steeper slope and a minimum at $x_{100} \sim 1.3$. Nevertheless, the calculated curve still differs substantially from the experimental result. The calculated curves have used Dexter's result[27] $\alpha_\perp/\alpha_\parallel = 2.123$. This ratio yields a slope

$$\{[1/\alpha_D(0)][d\alpha_D(x)/dx']\}_{x'=0} = -0.0714$$

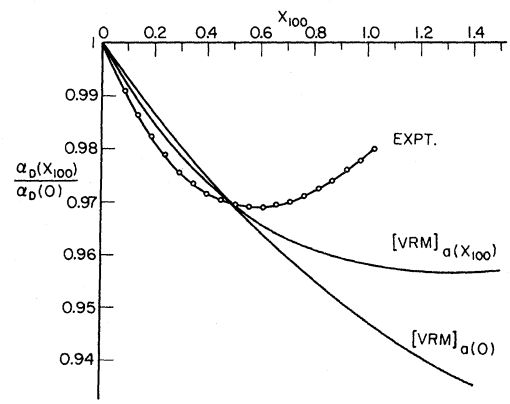

FIG. 10. The relative strain-dependent donor polarizability experimental results for $\alpha_D(x_{100})/\alpha_D(0)$ for sample $P5$ (see Fig. 7) are compared with theoretical calculations based on (1) the valley repopulation model (VRM) only and (2) the VRM with a strain-dependent valley envelope function Bohr radius $a_j(x_{100})$. The latter calculation does produce a minimum at about $x_{100} \sim 1.32$.

from Eq. (14) which is slightly more than half the slope for the P donors. If one increases the ratio $\alpha_\perp/\alpha_\parallel$ to 3.7 one can fit the initial slope for the Si: P results, but the minimum is pushed out to $x_{100}^{\min} \sim 2.0$ and one obtains overall poorer agreement with the experimental curve. This strongly suggests the theoretical expression is inadequate and some physical contribution is missing from the theory. This will be treated more carefully in the following paper. One obvious correction to include is the strain dependence of the valley-valley coupling parameter Δ. With strain-dependent valley Bohr radii $a_j(x)$ one logically expects the valley-valley matrix elements Δ_{ij} to be strain dependent. Since these matrix elements depend critically on the central-cell potential and the core portion of the donor wave function they are very difficult to reliably calculate. Here, we will adopt an empirical approach and assume a single $\Delta(x')$ with a power series of the form

$$\Delta(x') = \Delta(0)(1 + C_1 x' + C_2 x'^2 + C_3 x'^3 + \cdots).$$

The $\alpha_D(x_{100})/\alpha_D(0)$Si: P results in Fig. 10 can be fit very well with $C_1 = 0.101$, $C_2 = -0.236$, and $C_3 = 0.068$. This $\Delta(x')$ leads to a ground-state donor energy $E_{GS}(x')$ different than that given in Wilson and Feher. $E_{GS}(x')$ becomes more negative up to $x' \sim 0.38$ [where $E_{GS}(0.38) = 1.0039\, E_{GS}(0)$] then increases until $E_{GS}(1.1) = 0.995\, E_{GS}(0)$. This decrease in binding energy for $x' > 0.38$ is consistent with the increasing value of $\alpha_D(x_{100})/\alpha_D(0)$ for $x' > x_{100}^{\min}$.

In Fig. 11 the [110] axis experimental results for $\alpha_D(x_{110})/\alpha_D(0)$ are compared with the theoretical expressions from Eqs. (11) and (10) [see Eq. (A1)] for $\alpha_D(x_{100})/\alpha_D(0)$. Again $\alpha_\perp/\alpha_\parallel$ has been set equal to Dexter's[27] calculated ratio of 2.123. The $[\mathrm{VRM}]_{a(0)}$ curve has too small a slope, while the $[\mathrm{VRM}]_{a(x_{110})}$ curve is somewhat better, but still not in good agreement with the data. The smaller range of x_{110} makes it less fruitful to consider the specific form of $\Delta(x)$ as was done for the [100] axis case.

For the Sb donor results shown in Fig. 9 the data for $\alpha_D(x_{100})/\alpha_D(0)$ can again be well fit with a strain-dependent $\Delta(x')$, with $C_1 = -0.0527$, $C_2 = +0.023$, $C_3 = -0.037$, and $C_4 = 0.016$. This $\Delta(x')$ leads to a slightly different $E_{GS}(x')$ behavior than for the P donor. Because of the strong donor dependence of the valley-valley coupling parameters it is not surprising that the strain-dependent $\Delta(x')$ would also be different for the different donors.

E. Zero-stress donor polarizabilities

The effective donor polarizabilities $\alpha_D(N_D, T, x = 0)$ calculated using Eq. (12) are shown in Fig. 12 vs T for a group of Si: P samples. These effective $\alpha_D(N, T, x = 0)$ contain a hopping contribution. This hopping contribution can be largely eliminated either (1) by performing a Kramer's-Kronig analysis on the $\epsilon(N_D, T, x = 0, \omega)$ data to extract ϵ_∞ [given by Eq. (1) with $\alpha_D(N_D, T = 0)$], or (2) by extrapolating the data for $\alpha_D(N_D, T, x = 0)$ to $T = 0$ K. Figure 12 shows a much steeper temperature dependence for $\alpha_D(T)$ for sample $P2$. This sample may be more heavily compensated than the more heavily doped samples and also appears to have a larger hopping activation energy than the more heavily doped Si samples.

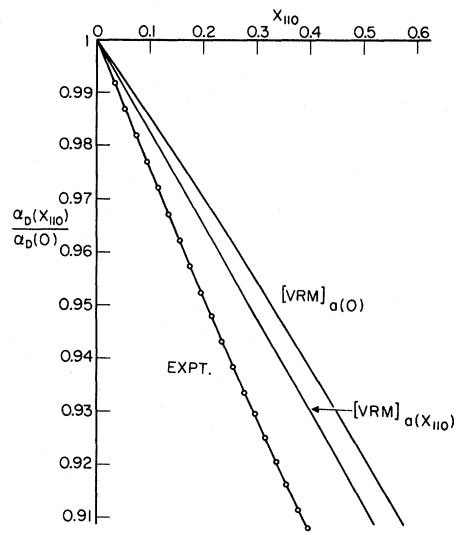

FIG. 11. The relative strain-dependent donor polarizability experimental results for $\alpha_D(x_{100})\alpha_D(0)$ for sample $P6$ (see Fig. 8) are compared with (1) the valley repopulation model (VRM) only and (2) the VRM with a strain-dependent valley envelope function Bohr radius $a_j(x_{110})$.

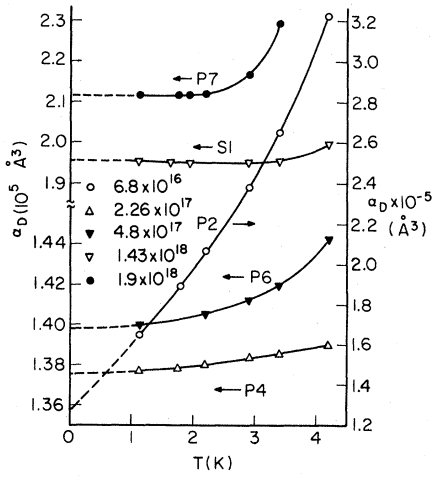

FIG. 12. The zero-strain polarizabilities $\alpha_D(x = 0, T)$ for a group of Si: P samples versus temperature. The extrapolated $T \to 0$ α_D values are given in Table III. Note the different scales for different samples.

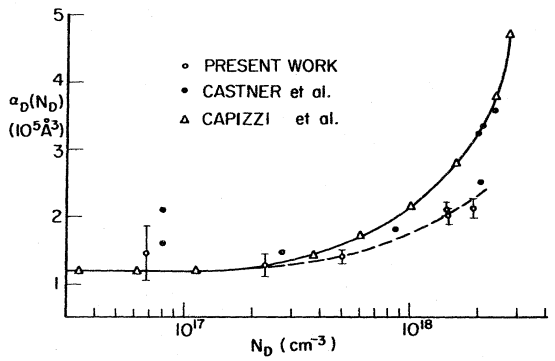

FIG. 13. The P-donor polarizability $\alpha_D(N_D, T \to 0\ \mathrm{K})$ versus donor concentration from the present work Φ; from Castner *et al.* (Ref. 12) •; from Capizzi *et al.* (Ref. 13) △.

This latter conclusion is in good agreement with the Ge:Sb results of Fritzsche.[52] Fritzsche's results show the ϵ_3 activation energy reaching a broad maximum for $N_D \sim 8 \times 10^{15}$ cm^{-3} ($N_D \sim 0.04 N_c$) and falling very rapidly for $N_D > N_c/5$. Sample P_2 ($N_D = 6.8 \times 10^{16}$, $N_D \approx 0.02 N_c$) lies near the peak in ϵ_3 for these Si:P samples. Samples *P*7 and *S*1 show considerably smaller slopes for $T < 2.5$ K while *P*6 and *P*4 show relatively small slopes (note the scale change for these samples) and are thought to be very weakly compensated. The data in Fig. 12 is extrapolated to $T = 0$ K to obtain values of $\alpha_D(N_D, T = 0, x = 0)$ which are listed in Table III.

The concentration dependence of $\alpha_D(N_D, T = 0, x = 0)$ for Si:P inferred from the data and Eq. (12) is shown in Fig. 13 and compared with earlier work. In the dilute limit ($N_D \lesssim 5 \times 10^{17}$ cm^{-3}) the present results agree with the more accurate results of Capizzi *et al.*[13] reasonably well. However, the samples at concentrations 1.43×10^{18}/cm^3 and 1.9×10^{18}/cm^3 have $\alpha_D(N_D, T = 0)$ values approximately 30% below the previous data. The reason for these lower values is not understood, but these samples are from Czochralski-grown ingots with substantial amounts of oxygen. Furthermore, the compensation in these particular samples may be larger than in the samples studied in previous work. The effect of compensation is to increase N_c and to decrease $\epsilon(N_D)$ at a given value of neutral donor concentration ($N_D - N_A$). However, the present data does support the idea of a donor polarizability enhancement as $N_D \to N_c$. Although the error in α_D is large for the 6.8×10^{16}/cm^3 sample, the extrapolation of the $\alpha_D(N_D)$ data to small values yields $\alpha_D(0) = (1.2 \pm 0.2) \times 10^5$ Å^3 for the isolated P donor. This is in excellent agreement with the value $\alpha_D(0) = (1.15 \pm 0.1) \times 10^5$ Å^3 determined by Capizzi *et al.*[13] Lipari and Dexter[53] have calculated $\alpha_D(0) = 1.2 \times 10^5$ Å^3 for the P donor in Si using an isotropic envelope function containing many different exponentials with a substantial spread in Bohr radii. The Sb-doped Si samples studied in this work (all dilute) yield a value $\alpha_D(0) = (1.9 \pm 0.6) \times 10^5$ Å^3 for the Sb donor. This is in reasonable agreement with the calculated value[53] (neglecting anisotropy) of $\alpha_D(0) = 1.6 \times 10^5$ Å^3.

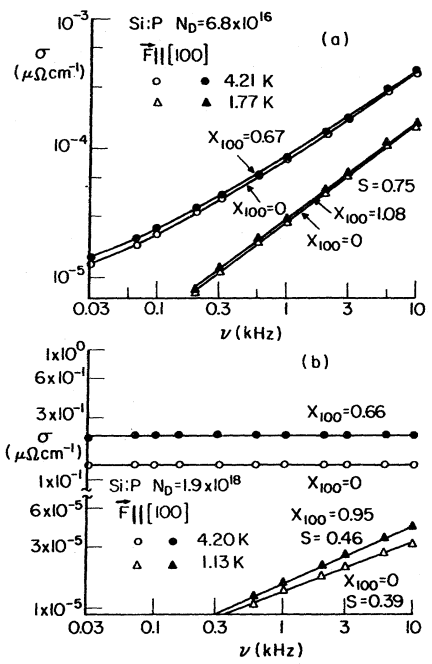

FIG. 14. The ac conductivity $\sigma(T, x, \nu)$ versus frequency ν for $T = 4.2$ K and a lower temperature for zero strain and for a large strain, x_{100}, along a [100] axis. (a) Sample *P*1 (Si:P, $N_D = 6.8 \times 10^{16}$ cm^{-3}); (b) sample *P*7 (Si:P, $N_D = 1.9 \times 10^{18}$ cm^{-3}).

F. Stress-dependent ac conductivity

Figure 14 shows the frequency-dependent conductivity $\sigma(N_D, T, x, \omega)$ for a dilute sample (a) and for a concentrated sample (b) for $x_{100} = 0$ and for a large value of x_{100}. The dilute sample exhibits characteristic hopping behavior ($\sigma \alpha \omega^s$) and shows a small increase of σ with x which is in agreement with the Bohr radius increase and polarizability increase for $x_{100} > x_{100}^{\min}$. The increase is slightly larger at low frequencies for the 4.21-K data. There appears to be no significant strain-dependent change in the slope s. The temperature dependence for $\nu > 1$ kHz is approximately linear. The highly doped sample ($N_D \sim 1.9 \times 10^{18}$/cm^3) in (b) shows a much stronger temperature dependence and a much bigger strain-dependent $\sigma(T, x, \omega)$. At 4.2 K the conductivity is flat ($\sigma \propto \nu^0$), characteristic of the dc value. The ratio $\sigma(x_{100}$

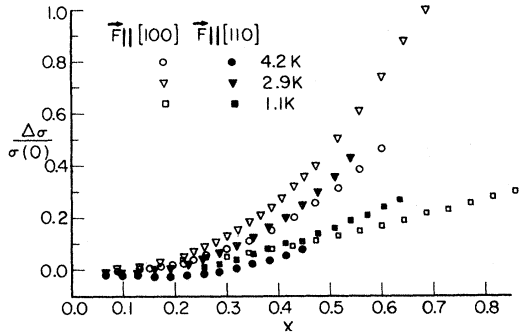

FIG. 15. The normalized piezoconductivity shift $[\sigma(x)-\sigma(0)]/\sigma(0)$ versus the reduced valley strain x for three temperatures for the stress along [100] and [110] axes. All the data is taken for the frequency $\nu=3.0$ kHz. The data are from Si:P samples $P9$ and $P10$.

$=0.66)/\sigma(x_{100}=0)\approx 1.68$. At the lower temperature $T=1.13$ K the two $\sigma(\omega,x)$ curves are not parallel and show different slopes, namely, $s\approx 0.39$ for $x_{100}=0$ and $s=0.46$ for $x_{100}=0.95$. The change $\sigma(x)/\sigma(0)$ is substantially smaller than at 4.2 K. Figure 15 shows the relative change $[\sigma(x)-\sigma(0)]/\sigma(0)$ vs x (at $\nu=3$ kHz) for two Si:P samples, a [100] axis and [110] axis sample. The [110] axis data show a slight negative dip before increasing, while the [100] data are flat (or small) before increasing. The lowest temperature data show the [110] and [100] axis data crossing at about $x=x'\sim 0.4$, unlike the higher temperature data.

The above data will not be quantitatively analyzed, but it is in qualitative agreement with the ac hopping conductivity model of Pollak and Geballe[35] and the dc piezoconductance model developed for hopping by Fritzsche.[6]

V. SUMMARY AND CONCLUSIONS

The strain-dependent behavior of the low-temperature dielectric constant of high-purity Si is consistent with the earlier hydrostatic pressure results of Cardona *et al.*[24] The value $\epsilon_h(T\to 0)=11.4\pm 0.06$ obtained for pure Si is in excellent agreement with the value 11.4 ± 0.05 inferred by Faulkner[28] from the energy positions of the $2p$ and $3p$ donor states. The strain-dependent results for the doped samples show behavior for the [100] and [110] stress axes that is apparently different, and also differs substantially from the prediction of the valley repopulation model, including the Fritzsche prescription for the valley and strain-dependent Bohr radii. The empirical approach of introducing a strain-dependent valley-valley coupling matrix $\Delta(x')$ can be utilized to explain the features of the [100] stress-axis data. The following paper presents a new approach to the theory of the strain-dependent donor polarizability which is somewhat different in approach and which can consistently explain both the [110] and [100] axis-strain data for Si:P.

One possibly surprising result is the relatively small concentration dependence of the strain-dependent behavior of $\alpha_D(N_D,x)$ for Si:P. Over a concentration range from $6\times 10^{16}/\text{cm}^{-3}$, where isolated donor behavior should dominate, to $1.9\times 10^{18}/\text{cm}^{-3}$, where pairs and larger donor clusters might be expected to dominate, the strain dependence of $\alpha_D(N_D,x)$ changes relatively little with less than 20% changes in slope and depth of the [100] axis minimum, although there is almost a 50% change in the position of the (100) minimum $x_{100}^{\min}$. This suggests either (1) that the strain-dependent behavior of clusters is very similar to that of isolated donors, or (2) that the importance of clusters near $N\approx N_c/2$ is less than previously thought.

The P-donor polarizability obtained in the dilute limit is in good agreement with the experimental value obtained by Capizzi *et al.*[13] and the calculated value obtained by Lipari and Dexter.[53] The concentration dependence of $\alpha_D(N_D,x=0)$ found is less than that obtained in previous work, possibly because of larger compensation. However, the data does show a donor polarizability enhancement as $N_D\to N_c$. More work is clearly required to establish the effect of compensation on the dielectric anomaly for (N_D-N_A) slightly less than N_c.

ACKNOWLEDGMENT

This work was supported in part by an NSF Grant No. DMR77-20450.

APPENDIX: STRAIN-DEPENDENT POLARIZABILITIES

Employing Eqs. (10), (5), and (8) and the parameters given in Table I for P donors in Si one can obtain $\alpha_D(x_{110})$ for these donors. A series expansion in x_{110} yields for P

$$\frac{\alpha_D(x_{110})}{\alpha_D(0)}=(1-0.1732x_{110}-0.0155x_{110}^2+0.0190x_{110}^3+\cdots). \tag{A1}$$

To obtain these results we have used $\alpha_D(0)=\frac{1}{3}(\alpha_\parallel+2\alpha_\perp)$ and $\alpha_\perp/\alpha_\parallel=2.123$ obtained by Dexter.[27] Using Eqs. (13), (5), and (8) and the parameters in Table I for P donors, one obtains for the [100] axis-stress case the results

$$\frac{\alpha_D(x_{100})}{\alpha_D(0)}=(1-0.0866x_{100}+0.0560x_{100}^2-0.0082x_{100}^3+\cdots). \tag{A2}$$

The results for Sb donors are virtually identical

with the results in Eqs. (A1) and (A2). The expressions for the ground-state donor energy to be used in Eq. (5) are given by

$$E_{GS}(x_{110}) = E_{EMA} - \Lambda - \Delta\left(2 + \delta + \frac{x_{110}}{2} - \frac{3}{2}\left(x_{110}^2 - \tfrac{4}{3}x_{110} + 4\right)^{1/2}\right) \tag{A3}$$

and

$$E_{GS}(x_{100}) = E_{EMA} - \Lambda - \Delta\left(2 + \delta - \frac{x_{100}}{2} - \frac{3}{2}\left(x_{100}^2 + \tfrac{4}{3}x_{100} + 4\right)^{1/2}\right). \tag{A4}$$

In the treatment presented in this paper the single-valley correction Λ to $E_{GS}(x)$ is considered to be independent of stress. Only the adjacent valley-valley coupling matrix element Δ is considered to vary with x' in obtaining an empirical fit of $\alpha_D(x')/\alpha_D(0)$.

---

*Based in part upon a dissertation submitted in partial fulfillment of the degree requirements for the Doctor of Philosophy at the University of Rochester.

†Present address: 1, Lorong Tiong Nam 6, Kuala Lumpur 02-08, Malaysia.

[1]R. J. Sladek, J. Phys. Chem. Solids 8, 515 (1959).

[2]O. Beckman, E. Hanamura, and L. J. Neuringer, Phys. Rev. Lett. 18, 773 (1967).

[3]D. Ferre, H. Dubois, and G. Biskubski, Phys. Status Solidi B 70, 81 (1975).

[4]M. Pepper, Philos. Mag. B 37, 187 (1978).

[5]See the review by H. G. Drickamer, in *Solid State Physics*, edited by F. Seitz and D. Turnbull (Academic, New York, 1965), Vol. 17, p. 1.

[6]H. Fritzsche, Phys. Rev. 125, 1552 (1962); 125, 1560 (1962); M. Cuevas and H. Fritzsche, Phys. Rev. 137, A1847 (1965); 139, A1628 (1965).

[7]V. V. Kolomoets, A. V. Fedosov, and V. P. Shapovalov, Fiz. Tekh. Poluprovodn 10, 1390 (1976) [Sov. Phys.-Semicond. 10, 824 (1976)]; V. V. Kolomoets and A. V. Fedosov, *ibid.* 10, 2043 (1976) [10, 1219 (1976)].

[8]A. A. Kastalskii, S. B. Maltev, and B. Yu Vengalis, Fiz. Tverd. Tela 18, 2201 (1976) [Sov. Phys.-Solid State 18, 1282 (1976)].

[9]H. F. Staunton and F. H. Pollak, Phys. Lett. 25A, 751 (1967).

[10]T. G. Castner, N. K. Lee, G. S. Cieloszyk, and G. L. Salinger, Phys. Rev. Lett. 34, 1627 (1975).

[11]P. Townsend, J. Phys. C 11, 1481 (1978).

[12]T. G. Castner, N. K. Lee, H. S. Tan, L. Moberly, and O. Symko, J. Low Temp. Phys. 38, 447 (1980).

[13]M. Capizzi, G. A. Thomas, F. DeRosa, R. N. Bhatt, and T. M. Rice, Phys. Rev. Lett. 44, 1019 (1980).

[14]C. S. Smith, Phys. Rev. 94, 42 (1954).

[15]R. W. Keyes, in *Solid State Physics*, edited by F. Seitz and D. Turnbull (Academic, New York, 1960).

[16]H. Fritzsche, in *The Metal Non-Metal Transition in Disordered Systems*, edited by L. R. Friedman and D. P. Tunstall (SUSSP, Edinburgh, 1978).

[17]J. A. Chroboczek, Philos. Mag. 42, 933 (1980).

[18]D. K. Wilson and G. Feher, Phys. Rev. 124, 1068 (1961).

[19]E. B. Hale and T. G. Castner, Phys. Rev. B 1, 4763 (1970).

[20]D. W. Olson and T. G. Castner, Phys. Rev. B 17, 3318 (1978).

[21]J. C. Hensel, H. Hasegawa, and M. Nakayama, Phys. Rev. 138, A225 (1965).

[22]I. Balslev, Phys. Rev. 143, 636 (1966).

[23]R. L. Aggarwal and A. K. Ramadas, Phys. Rev. 137, A602 (1965); 140, A1246 (1965).

[24]M. Cardona, W. Paul, and H. Brooks, *Proceedings of the International Conference on Solid State Physics in Electronics and Telecommunications, Brussels, 1958* (Academic, New York, 1960); J. Phys. Chem. Solids 8, 204 (1959).

[25]P. J. Price, Phys. Rev. 104, 1223 (1956).

[26]J. Bethin, T. G. Castner, and N. K. Lee, Solid State Commun. 14, 1321 (1974).

[27]D. L. Dexter, in *Proceedings of 13th International Semiconductor Conference, Rome, 1976*, edited by F. G. Fumi (North-Holland, Amsterdam, 1977), p. 1137.

[28]R. A. Faulkner, Phys. Rev. 184, 713 (1969).

[29]T. G. Castner, Phys. Rev. Lett. 8, 13 (1962); Phys. Rev. 155, 816 (1967).

[30]See, for example, J. F. Nye, *Physicsl Properties of Crystals* (Oxford University Press, London, 1957), Chap. 8.

[31]C. Herring and E. Vogt, Phys. Rev. 101, 944 (1956).

[32]E. B. Hale, J. Phys. Chem. Solids 34, 621 (1973).

[33]J. J. Hall, Phys. Rev. 161, 756 (1967).

[34]G. W. Castellan and F. Seitz, *Semiconducting Materials* (Butterworths, London, 1951), p. 8.

[35]M. Pollak and T. H. Geballe, Phys. Rev. 122, 1742 (1961).

[36]H. R. Hasse, Proc. Cambridge Philos. Soc. 26, 542 (1930).

[37]J. Swartzendruber, N. B. S. Technical Note 199, unpublished.

[38]F. M. Smits, Bell Syst. Tech. J. 37, 711 (1958).

[39]F. Mousty, P. Ostoja, and L. Passari, J. Appl. Phys. 45, 4576 (1974).

[40]S. M. Sze and J. C. Irvin, Solid State Electron. 11, 599 (1968).

[41]D. W. Olson, Ph.D. thesis, University of Rochester, 1969, unpublished.

[42]A. H. Scott and H. L. Curtis, J. Res. Nat. Bur. Stand. 22, 747 (1939).

[43]S. M. Sze, *Physics of Semiconductor Devices* (Wiley, New York, 1969), Chap. 8, p. 371.

[44]J. Van Vechten, Phys. Rev. 182, 891 (1969).

[45]H. W. Briggs, Phys. Rev. 77, 287 (1950).

[46]W. Primak, Appl. Opt. 10, 759 (1971).

[47]C. D. Salzberg and J. J. Villa, J. Opt. Soc. Am. 47, 244 (1957).
[48]F. Lukes, J. Phys. Chem. Solids 11, 342 (1959); Czech. J. Phys. B 10, 317 (1960).
[49]J. J. Villa, Appl. Opt. 11, 2102 (1972).
[50]H. W. Icenogle, B. C. Platt, and W. L. Wolfe, Appl. Opt. 15, 2348 (1976).
[51]W. C. Dunlap, Jr. and R. L. Watters, Phys. Rev. 92, 1396 (1953).
[52]H. Fritzsche, J. Phys. Chem. Solids 6, 69 (1958).
[53]N. O. Lipari and D. L. Dexter, Phys. Rev. B 18, 1346 (1978).